Microwave Engineering
Ulm University

ulm university universität ulm

Synchronization of Radar Sensors in a Network Based on Inter-Sensor Interference

Maximilian Steiner, Manuel Keller, Johanna Geiß, Martin Vossiek, and Christian Waldschmidt

DOI:

Synchronization of Radar Sensors in a Network Based on Inter-Sensor Interference

Maximilian Steiner*, Manuel Keller*, Johanna Geiß#, Martin Vossiek#, and Christian Waldschmidt*
*Institute of Microwave Engineering, Ulm University, 89081 Ulm, Germany
#Institute of Microwaves and Photonics, Friedrich-Alexander-Universität Erlangen-Nürnberg (FAU), Erlangen, Germany
Email: Maximilian.Steiner@uni-ulm.de

***Abstract*— In networks of distributed radar sensors the measurements need to be synchronized to enable a joint processing and to avoid interference between the nodes. The proposed approach supersedes the distribution of a dedicated trigger cable by utilizing the multistatic target responses for time synchronization of the nodes. Each node is operated with a chirp-sequence modulation scheme, and the initial measurements are free running. The time-shifts between all sensors are recovered from the mutual interference of the nodes. The approach is verified by measurements that are conducted with three sensors, operated in the 77 GHz frequency band.**

I. Introduction

Millimeter-wave radars are currently the state of the art for localization applications. The small-sized sensors provide a high performance, which makes networks of multiple radar sensors attractive. In the automotive sector a rapid increase of radars on a single car can be observed pointing towards a 360°-perception of the environment. The same is valid for the growing field of robotics, which for instance includes autonomous robots for transportation tasks, service robots, or rescue robots. The optimal use of multiple sensors on the same platform with regard to a joint evaluation demands a proper management of resources like time and bandwidth. Ideally, all radar sensors are operated using a maximum allowed bandwidth in terms of high range separability. A joint processing of multiple sensors measurements also requires a simultaneous acquisition. To optimize both factors time synchronization is a crucial concept.

Usually, a trigger signal is distributed to all sensors to guarantee simultaneous measurements [1]. Secondary radar approaches with special hardware achieve wireless synchronization between active nodes requiring line-of-sight (LoS) conditions [2],[3]. In contrast, the approach proposed in this paper retrieves time-synchronized measurements within a network of standard chirp-sequence radar sensors. This does not require an LoS, as the bistatic interference signals are utilized to estimate the temporal shifts between the free-running sensor measurements.

II. System Setup

The proposed system uses very simple single-channel radar sensors. They operate with a chirp-sequence modulation [4] that allows to estimate the range and radial velocity of a detected target.

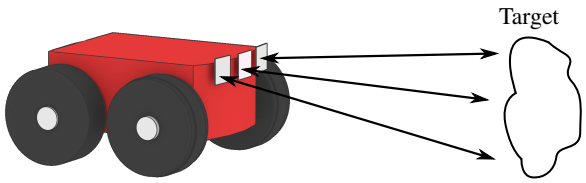

Fig. 1. Exemplary spatial distribution of three sensors on a robot.

Multiple sensors are spatially distributed on a platform, e.g., a robot or a car. The sensors are mounted side-by-side, so that at least 2 sensors cover a common field-of-view (FoV) to enable the use of multilateration techniques [5], [6] for target localization. It is assumed that no LoS paths between the nodes exists, due to the orientation of the sensors. Hence, bistatic paths between the nodes only exist when scattering at targets within a common FoV occurs.

The chirp-sequence modulation scheme consists of rising, falling, and continuous frequency modulated parts. All nodes operate with independently generated signals using the same modulation parameters. Under consideration of synchronous measurements, the center frequencies of all sensors are shifted respectively to avoid interference among sensors in the network. Hence, independent monostatic radar measurements of a common scene can be achieved by the time synchronized system. Only a data connection between each sensor and a central processing unit is set up to capture the measurement data and to configure the radar sensors.

Further, a rough software trigger is used to start the measurements of each sensor. A low jitter time as well as the absolute delays between the nodes are crucial for interference-free measurements, but sufficiently low inter-sensor delays can hardly be obtained in data networks that allow high data throughput. The timings of the transmitted modulation scheme are determined by an FPGA-based state-machine, which depends on a local oscillator. This allows for chirp-sequence transmissions with reproducible timings and also for arbitrary configurable intervals between 2 sequences.

III. Signal Model

In the following the signal model of the system is derived with respect to the intended interference between the networked radar nodes. The transmitted chirp-sequence signals

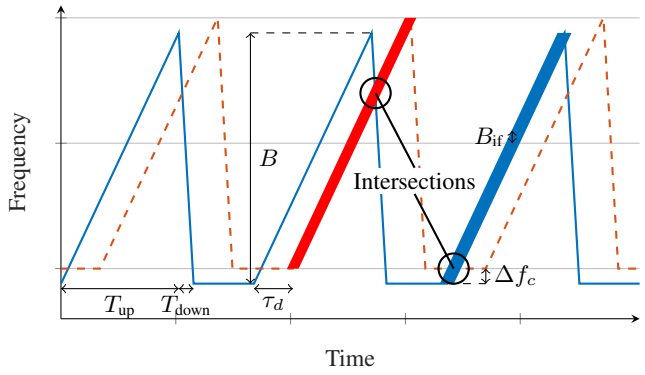

Fig. 2. Exemplary chirp modulation of two interfering sensors, sensor 1 (blue) and sensor 2 (red, dashed). The marked intersections result in the interfered time slots T_{int}.

of 2 sensors are exemplarily depicted in Fig. 2. The signals are shifted undesirably in time by a delay τ_d and have an intended frequency offset Δf_c. On the receiver side the up-ramp part of the respective sensor signal is considered, which can be expressed by the phase term

$$\varphi(t) = 2\pi \int_{-T/2}^{t} \left(f_c + mt\right)\mathrm{d}t = 2\pi\left(f_c t + \frac{m}{2}t^2\right) - \varphi_0 \quad (1)$$

as described in [7]. Here, m denotes the slope in $^{\text{Hz}}/_{\text{s}}$, which is determined by the RF bandwidth B and the ramp duration T_{up}. After reception of an FMCW ramp with the same slope and the same center frequency f_c, the down-converted signal phase depends only on the shift in time τ resulting in

$$\Delta\varphi(t,\tau) = \varphi(t) - \varphi(t-\tau) = 2\pi\left(f_c\tau + mt\tau - \frac{m}{2}\tau^2\right). \quad (2)$$

In a monostatic measurement of a stationary target with the distance R, τ is given by the time-of-flight (ToF) between the sensor and the target

$$\tau_{\text{tar}} = \frac{2R}{c}. \quad (3)$$

Thus, the down-converted target response results in

$$\Delta\varphi_{\text{tar}}(t, f_c, m) = 2\pi\left(\frac{2f_cR}{c} + \frac{2mR}{c}t\right). \quad (4)$$

The delay of an interference signal over the bistatic path sums up to

$$\tau_{\text{int}} = \frac{2R}{c} + \tau_{\text{d}} = \tau_{\text{tar}} + \tau_{\text{d}} \approx \tau_{\text{d}}, \quad (5)$$

assuming that the sensor spacing is small compared to the target distance. For not synchronized measurements, it can also be assumed that the ToF is negligible, since the measurement delay is usually much higher. Further, the IF filter bandwidth B_{if} of typical automotive radar systems amounts to only a few percent of the transmitted RF bandwidth. This reduces the detectable interference to a short time

$$T_{\text{int}} = \frac{B_{\text{if}}}{m - m_{\text{int}}} \quad (6)$$

at which the transmitted signal with the slope m crosses the interfering frequency ramp with a slope m_{int}. Hereby, m_{int} represents the actual slope of the interferer, which can be either 0 or -($^{B}/_{T_{\text{down}}}$), as depicted in Fig. 2.

With the assumption of (5) the received signal phase for these time slots is given by

$$\begin{aligned}\Delta\varphi_{\text{int(1,2)}} &= \varphi_1(t) - \varphi_2(t-\tau)\\ &= \Delta\varphi_{\text{tar}}(t, f_{c,2}, m_2) + 2\pi\Big[\Delta f_c t + \frac{1}{2}(m_1 - m_2)t^2\\ &+ f_{c,2}\tau_{\text{d}} - \frac{m_2 R}{c}\tau_{\text{d}} - \left(m_2\tau_d + \frac{m_2 v\tau_{\text{d}}}{c}\right)t\Big] + \Delta\varphi_0\\ &\approx 2\pi\left[\Delta f_c t + \frac{1}{2}(m_1 - m_2)t^2 + f_{c,2}\tau_{\text{d}} - m_2\tau_{\text{d}}t\right] + \Delta\varphi_0. \quad (7)\end{aligned}$$

The short time interference can be divided into 2 basic types for the proposed system, which comprises sensors with equal modulations, but with slightly shifted center frequencies as shown in Fig. 2. At first, the sampled rising ramp might be interfered by a continuous wave (CW) signal that is sent in the break between a down- and the following up-ramp, called a break interference. Further, the up-ramp can be interfered by a falling ramp, which is referred to as down-ramp interference. The impact on the time domain samples of both is shown in Fig. 3 for a simulated example with 2 sensors. There is a small chance that the interference lies within the IF bandwidth of the receiving sensor. In this case, all samples either from a break interference to the end of the sampled ramp or from its beginning to a down-ramp interference would be affected. This option is called inband interference.

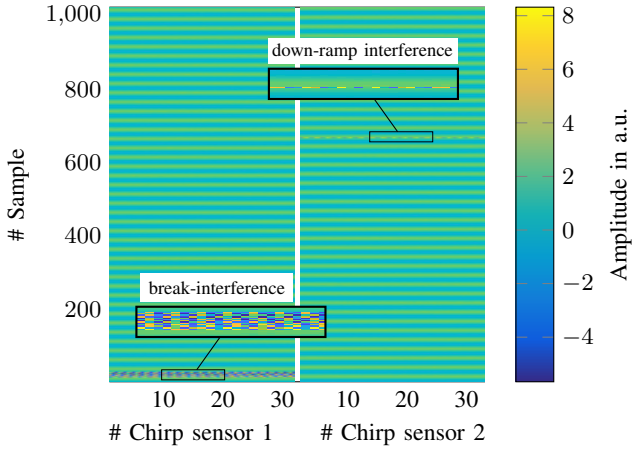

Fig. 3. Simulated mutual interference of two sensors in time domain (fast time in samples, slow time in chirps). Chirp modulation according to Fig. 2: sensor 1 (left), sensor 2 (right).

IV. Algorithm for Delay Calculation

In the following all steps regarding the synchronization as shown in Fig. 4 are explained in detail.

A. Interference detection and classification

In order to calculate the delay of each sensor, it is necessary to extract the interfered samples from the raw time-domain data. It can be assumed, that the interference always occurs in the same sample for every chirp and thus represents a horizontal line across the whole chirp sequence within our time-domain data matrix as shown in Fig. 3. Measurements show that its sampled amplitude changes from chirp to chirp,

while the responses of static targets remain constant. By subtracting the data of the previous ramp, these clutter and target responses within each chirp can be decimated. After that the lines of interfered samples are emphasized, as depicted in Fig. 5, and can be extracted by using a simple CFAR-peak detection [8]. A sample is considered interfered, if the number of CFAR detections across all chirps is higher than 80 % of the total number of chirps in one sequence. Measurements show that the successful detection of an interference depends highly on its incident power. As the following parts of the algorithm have to comply the found interfered samples, both missing and wrong detections can lead to critical errors in the delay calculation.

After detecting the interferences they need to be classified as either break- or down-ramp interference. The following criteria holds for a break interference:

$$f_{\text{int,1}} - f_{\text{min,1}} \approx \Delta f_c, \tag{8}$$

where $f_{\text{int,1}}$ is the frequency of the interfered sample of the current sensor, $f_{\text{min,1}}$ its minimum frequency, and Δf_c the frequency offset between the sensors. All samples that do not fulfill this criterion, are considered as down-ramp interferences. As an inband interference is very unlikely to occur, the algorithm does not consider this option any further. It can still find the delay of an affected node through the information provided by the other sensors. If this fails, the node is given a random time delay to create a different constellation in the next iteration.

B. Utilization of the interference types to find delays

The described interference types show properties that contribute in different ways to achieving the goal of measurement synchronization. For the direct calculation of the delay between 2 nodes, only down-ramp interferences are useful. The intersection point of the ramps is related to a single frequency, which can be found both in the up-ramp of the currently evaluated sensor and in the down-ramp of its opponent. For both nodes, the times from the chirp start point to this intersection can now be calculated. Their difference yields the delay τ_d. However, if there are multiple down-ramp interferences detected at the same sensor, like sensor 2 in Fig. 5, it is uncertain, which node causes which interference. Matching multiple down-ramp interferences to their causing nodes can be achieved, if the transmit order of the sensors is determined. Here, break interferences are useful, since through the distinct center frequency offsets of the sensors, the causing node is known (8). The sequence can be obtained by iterating through all sensor pairs (S_j, S_k) and evaluating their interferences the following way:

- Break interference in S_j by S_k: $t_{\text{start,j}} < t_{\text{start,k}}$,
- Down-ramp interference in S_j by S_k: $t_{\text{start,k}} < t_{\text{start,j}}$,

As it can be seen in Fig. 2, a sensor that receives a break interference always causes a down-ramp interference of its counterpart. Therefore, the matching of an interfered sample to the causing sensor can easily be done within these break-down ramp pairs. If no break interference is available, a down-ramp interference in combination with the correct timing sequence is sufficient for delay calculation.

C. Procedure and evaluation of the algorithm

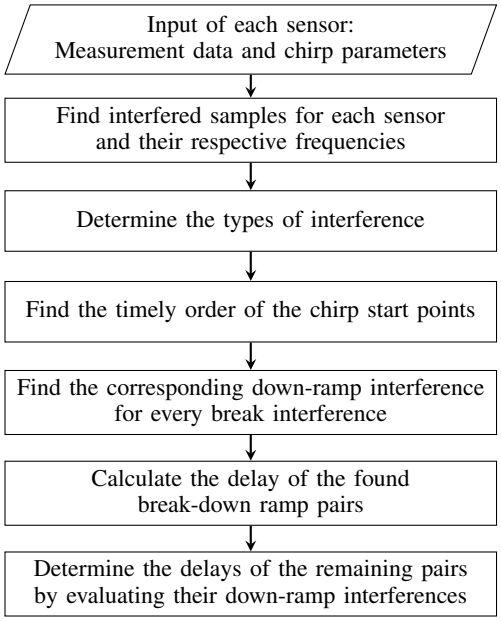

Fig. 4. Flowchart of the delay calculation algorithm.

The flowchart of the algorithm is shown in Fig. 4. First, the received data of the chirp-sequence is analyzed as described in Section IV-A to obtain the interfered samples. Their respective RF frequencies are determined using the knowledge of the chirp ramp pattern of the sensor, that maps each sample to its distinguished frequency (see Fig. 2). Next, the found interfered samples are classified by using the criteria in IV-A. Knowing all the interference possibilities, the algorithm can determine the sequence of the chirp start points as described in Section IV-B. Afterwards, the respective delays can be determined starting off by calculating the delay of the break-down-ramp pairs and proceeding with the remaining down-ramp interferences. If the algorithm failed to obtain the delay for a node, it is set to a random value to create a different timing setup in the next measurement.

The algorithm was tested by creating 10 000 random delay values for each sensor. The interfered samples were determined by calculating the ramp intersections. Therefore, this evaluation method skips the finding of interferences within measured data and only tests the performance of the classification and delay calculation part. An individual case is solved, when the algorithm finds the predetermined delay of all nodes with a tolerance of four samples. Table 1 shows the result for up to six sensors, neglecting the trivial case of 2 nodes. All of them have the same chirp-modulation scheme as depicted in Fig. 2 and a node-to-node carrier frequency offset of 20 MHz. The results show that for 3 sensors the algorithm finds the delays instantly for the majority of cases. With increasing sensor count, the algorithm still finds solutions, but requires an increasing number of iterations to do so with

Table 1. Algorithm test results: solved cases (%) of 10 000 total cases with random delays.

Iteration	1	2	3	4	8	10
3 sensors	83.61	97.01	99.01	99.01	99.64	99.66
4 sensors	52.47	75.79	87.53	93.02	99.05	99.40
5 sensors	29.20	48.73	62.09	72.35	91.50	95.00
6 sensors	14.72	27.08	36.74	45.58	69.09	76.43

certainty. In the proposed scenario, it is, however, unlikely to have more than four side-by-side mounted sensors that can still detect the interferences of all the others.

V. Measurement Results

In order to verify the functionality of the whole synchronization approach, measurements for various delay constellations were performed using 3 sensors. In the following the results are presented.

The single sensors operated around the center frequencies $f_{c,1\ldots3}$ of 76.38 GHz, 76.42 GHz and 76.46 GHz, respectively, with a bandwidth of 1 GHz. Each up-ramp is sampled at a frequency $f_s = 4$ MHz, whereby an IF filter with a cut-off frequency $B_{if} = 7.5$ MHz was used. The measurements were conducted in a stationary scenario with 3 cylindrical targets at 1.35 m distance to the sensor plane. The sensors were displaced by 45 cm along a profile rail. In order to generate verifiable delays, an arbitrary waveform generator was used to start the measurements of the sensors.

The time-domain signals of all involved sensors are given in the lower part of Fig. 5, consisting of a sequence of 20 up-ramps respectively. Despite the low energy reflected by the target, the interfered samples after the subtraction step are clearly visible. The upper part of Fig. 5 shows a single chirp

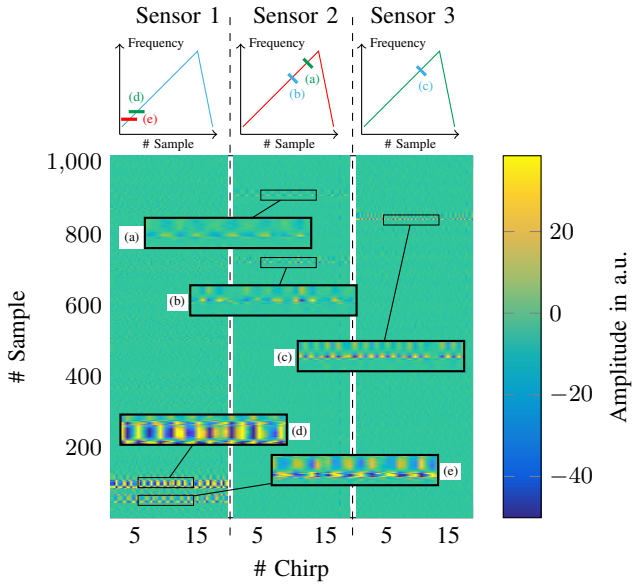

Fig. 5. Time domain data (fast time in samples, slow time in chirps) of 3 sensors in a multistatic measurement. Sensor 2 has a delay of 85 µs and sensor 3 a delay of 50 µs, each with respect to sensor 1.The interference effects (a)–(e) are visible and can be matched to their respective chirp intersections.

for each sensor and illustrates the points of mutual interference by crossing lines. Different labels mark the interfered samples respectively, whereby (a) to (c) are showing a down-ramp interference, while the labels (d) and (e) are each depicting a break interference.

Measurements comprising 6 different delay settings and 50 captured chirp-sequences in each case were conducted and evaluated using the proposed algorithm. The results of each set are presented in Table 2. The 6 delay constellations of the measurements show a slightly higher success rate in comparison to the simulation results for 3 sensors and a single iteration. A successful run results in a delay smaller than 1 µs.

Table 2. Bistatic measurement results with three sensors for various delay setups. Data was recorded for 50 chirp sequences.

Delay sensor 2 (µs)	40	60	85	335	380	400
Delay sensor 3 (µs)	100	360	50	385	360	50
Successful runs (%)	94	94	100	92	96	100

VI. Conclusion

The presented approach enables wireless synchronization of multiple radar sensors with the objective of a joint evaluation. The procedure does not rely on a dedicated synchronization wire or a line of sight between the sensors, but uses the standard chirp-sequence modulation scheme. The simulation results show a fast synchronization of 3 sensors within less than 3 iterations in 99 % of the cases. Measurements with 3 sensors and 3 targets were evaluated, showing comparably good results.

Acknowledgment

This work was funded by the German Research Foundation (DFG, Deutsche Forschungsgemeinschaft) – WA3506/11-1.

References

[1] R. Feger, C. Pfeffer, C. Schmid, M. Lang, Z. Tong, and A. Stelzer, "A 77-GHz FMCW MIMO Radar Based on Loosely Coupled Stations," in *The 7th German Microwave Conference (GeMiC)*, Mar. 2012.

[2] S. Roehr, P. Gulden, and M. Vossiek, "Precise Distance and Velocity Measurement for Real Time Locating in Multipath Environments Using a Frequency-Modulated Continuous-Wave Secondary Radar Approach," *IEEE Transactions on Microwave Theory and Techniques*, vol. 56, no. 10, pp. 2329–2339, Oct. 2008.

[3] M. Ash, M. Ritchie, K. Chetty, and P. V. Brennan, "A New Multistatic FMCW Radar Architecture by Over-the-Air Deramping," *IEEE Sensors Journal*, vol. 15, no. 12, pp. 7045–7053, Dec. 2015.

[4] A. G. Stove, "Linear FMCW radar techniques," *IEE Proceedings F — Radar and Signal Processing*, vol. 139, no. 5, pp. 343–350, Oct. 1992.

[5] M. Mirbach and W. Menzel, "A simple surface estimation algorithm for UWB pulse radars based on trilateration," in *IEEE International Conference on Ultra-Wideband (ICUWB)*, Sep. 2011, pp. 273–277.

[6] F. Fölster, H. Rohling, and U. Lubbert, "An Automotive Radar Network Based on 77 GHz FMCW Sensors," in *IEEE International Radar Conference*, May 2005, pp. 871–876.

[7] V. Winkler, "Range Doppler Detection for Automotive FMCW Radars," in *European Microwave Conference*, Oct. 2007, pp. 1445–1448.

[8] H. Rohling, "Radar CFAR Thresholding in Clutter and Multiple Target Situations," vol. AES-19, no. 4, July 1983, pp. 608–621.